PLOS | COMPUTATIONAL BIOLOGY

RESEARCH ARTICLE

Transient Accumulation of NO_2^- and N_2O during Denitrification Explained by Assuming Cell Diversification by Stochastic Transcription of Denitrification Genes

Junaid Hassan[1☯]*, Zhi Qu[1‡¤], Linda L. Bergaust[2‡], Lars R. Bakken[1☯]

1 Department of Environmental Sciences, Norwegian University of Life Sciences, Ås, Norway, **2** Chemistry, Biotechnology and Food Science, Norwegian University of Life Sciences, Ås, Norway

☯ These authors contributed equally to this work.
¤ Current address: College of Natural Resources and Environment, Northwest A&F University, Shaanxi, China
‡ ZQ and LLB also contributed equally to this work.
* junaid.hassan@nmbu.no

OPEN ACCESS

Citation: Hassan J, Qu Z, Bergaust LL, Bakken LR (2016) Transient Accumulation of NO_2^- and N_2O during Denitrification Explained by Assuming Cell Diversification by Stochastic Transcription of Denitrification Genes. PLoS Comput Biol 12(1): e1004621. doi:10.1371/journal.pcbi.1004621

Editor: Ilya Ioshikhes, Ottawa University, CANADA

Received: July 13, 2015

Accepted: October 22, 2015

Published: January 5, 2016

Data Availability Statement: All relevant data are within the paper and its Supporting Information files.

Funding: The manuscript is part of JH's PhD thesis at the Norwegian University of Life Sciences, which provided the funding together with the Norwegian Research Council. The funders had no role in study design, data collection and analysis, decision to publish, or preparation of the manuscript.

Competing Interests: The authors have declared that no competing interests exist.

Abstract

Denitrifying bacteria accumulate NO_2^-, NO, and N_2O, the amounts depending on transcriptional regulation of core denitrification genes in response to O_2-limiting conditions. The genes include *nar*, *nir*, *nor* and *nosZ*, encoding NO_3^--, NO_2^--, NO- and N_2O reductase, respectively. We previously constructed a dynamic model to simulate growth and respiration in batch cultures of *Paracoccus denitrificans*. The observed denitrification kinetics were adequately simulated by assuming a stochastic initiation of *nir*-transcription in each cell with an extremely low probability (0.5% h^{-1}), leading to product- and substrate-induced transcription of *nir* and *nor*, respectively, via NO. Thus, the model predicted cell diversification: after O_2 depletion, only a small fraction was able to grow by reducing NO_2^-. Here we have extended the model to simulate batch cultivation with NO_3^-, i.e., NO_2^-, NO, N_2O, and N_2 kinetics, measured in a novel experiment including frequent measurements of NO_2^-. *Pa. denitrificans* reduced practically all NO_3^- to NO_2^- before initiating gas production. The NO_2^- production is adequately simulated by assuming stochastic *nar*-transcription, as that for *nirS*, but with a higher probability (0.035 h^{-1}) and initiating at a higher O_2 concentration. Our model assumes that all cells express *nosZ*, thus predicting that a majority of cells have only N_2O-reductase (A), while a minority (B) has NO_2^--, NO- and N_2O-reductase. Population B has a higher cell-specific respiration rate than A because the latter can only use N_2O produced by B. Thus, the ratio $\frac{B}{A}$ is low immediately after O_2 depletion, but increases throughout the anoxic phase because B grows faster than A. As a result, the model predicts initially low but gradually increasing N_2O concentration throughout the anoxic phase, as observed. The modelled cell diversification neatly explains the observed denitrification kinetics and transient intermediate accumulations. The result has major implications for understanding the relationship between genotype and phenotype in denitrification research.

Author Summary

Denitrifiers generally respire O_2, but if O_2 becomes limiting, they may switch to anaerobic respiration (denitrification) by producing NO_3^--, NO_2^--, NO- and/or N_2O reductase, encoded by *nar*, *nir*, *nor*, and *nosZ* genes, respectively. Denitrification causes transient accumulation of NO_2^- and NO/N_2O emissions, depending on the activity of the four reductases. Denitrifiers lacking *nosZ* produce ~100% N_2O, whereas organisms with only *nosZ* are net consumers of N_2O. Full-fledged denitrifiers are equipped with all four reductases, genetic regulation of which determines NO_2^- accumulation and NO/N_2O emissions. *Paracoccus denitrificans* is a full-fledged denitrifying bacterium, and here we present a modelling approach to understand its gene regulation. We found that the observed transient accumulation of NO_2^- and N_2O can be neatly explained by assuming cell diversification: all cells expressing *nosZ*, while a minority expressing *nar* and *nir*+*nor*. Thus, the model predicts that in a batch culture of this organism, only a minor sub-population is full-fledged denitrifier. The cell diversification is a plausible outcome of stochastic initiation of *nar*- and *nir* transcription, which then becomes autocatalytic by NO_2^- and NO, respectively. The findings are important for understanding the regulation of denitrification in bacteria: product-induced transcription of denitrification genes is common, and we surmise that diversification in response to anoxia is widespread.

Introduction

The dissimilative reduction of nitrate (NO_3^-) to nitrite (NO_2^-), nitric oxide (NO), nitrous oxide (N_2O), and finally to N_2 (denitrification) is an indispensable process in the nitrogen cycle, returning N to the atmosphere as N_2. However, denitrification significantly leaks the gaseous intermediates NO and N_2O, both with serious consequences for the environment. N_2O catalyses depletion of the stratospheric ozone [1] and causes global warming, contributing ~10% to the anthropogenic climate forcing [2]. Data suggests that since the 1950s, the atmospheric N_2O has been increasing, and before being photolysed in the stratosphere, the gas persists for an average ~120 years in the troposphere [3]. ~70% of global N_2O emissions are tentatively attributed to microbial nitrification and denitrification in soils [4], where denitrification, generally, is considered a more dominant source [5].

To mitigate N_2O emissions, we need to understand the physiology of denitrifiers

To devise robust strategies for mitigating global N_2O emissions, a good understanding of its primary source is imperative, i.e., genetics, physiology, and regulatory biology of denitrifiers. Any knowledge of the environmental controllers of N_2O is incomplete without understanding the causal relationships of such controllers at the physiological level [6].

The biogeochemical models developed for understanding the ecosystem controls of denitrification and N_2O emissions treat the denitrifying community of soils and sediments as a single homogenous unit with certain characteristic responses to O_2 and NO_3^- concentrations [6,7]. Natural denitrifying communities, however, are mixtures of organisms with widely different denitrification regulatory phenotypes [8]. The regulatory response of such mixtures is not necessarily equal to the 'sum of its components' because there will be interactions, not the least, via the intermediates NO and NO_2^-. Hence, it is probably a mission impossible to predict the regulatory responses of complex communities based on their phenotypic composition.

Nevertheless, investigations of the regulation in model organisms like *Pa. denitrificans* provide us with essential concepts, enhancing our ability to understand the regulatory responses of mixed communities and to generate meaningful hypotheses. Thus, future biogeochemical models of N_2O and NO emissions are expected to have more explicit simulations of the regulatory networks involved, and a first attempt has recently been published [9].

Simulating the cell diversification in response to impending anoxia to analyse its implications for NO_2^-, N_2, and N_2O kinetics

Dynamic modelling has been used to a limited extent to analyse various denitrification phenotypes; for example, to analyse NO_3^- and NO_2^- reduction and gas-kinetic data for individual strains [10] and mixtures of selected phenotypes [11]; to model the consequence of competition for electrons between denitrification reductases [12,13]; to investigate the control of O_2 on denitrification enzymes and inhibition of cytochrome *c* oxidase by NO in *Agrobacterium tumefaciens* [14]; and to examine the effect of copper availability on N_2O reduction in *Paracoccus denitrificans* [15]. In our previous model [16], we simulated O_2 and N_2 kinetics from batch incubations of *Pa. denitrificans* [8,17] to test if a postulated cell diversification, driven by stochastic initiation of *nirS*, could explain the N_2 production kinetics in NO_2^--supplemented media. The available data also contained NO_3^--supplemented treatments but NO_3^- and NO_2^- were not monitored, and the experiment provided no information about the N_2O kinetics, except that the concentrations were extremely low (below the detection limit of the thermal conductivity detector used). Recently, a neat dataset was generated from batch incubations supplemented with NO_3^-, with frequent measurements of NO_2^- and a more sensitive detection of N_2O by an electron capture detector [18]. That encouraged us to extend our previous model and simulate the cell diversification during transition from oxic to anoxic conditions, targeting the regulation of Nar and *c*Nor/NosZ (N_2O emissions) in *Pa. denitrificans*.

Regulatory network of denitrification in *Paracoccus denitrificans*

Pa. denitrificans is a facultative anaerobe capable of reducing NO_3^- all the way to N_2:

$$NO_3^- \xrightarrow{\text{Nar}} NO_2^- \xrightarrow{\text{NirS}} NO \xrightarrow{c\text{Nor}} N_2O \xrightarrow{\text{NosZ}} N_2$$

In response to impending anoxic conditions, the organism sustains respiratory metabolism by producing the membrane-bound cytoplasmic nitrate reductase (Nar), cytochrome cd_1 nitrite reductase (NirS), cytochrome *c* dependent nitric oxide reductase (*c*Nor), and nitrous oxide reductase (NosZ). Transcription of the genes encoding these reductases (*narG*, *nirS*, *norBC*, and *nosZ*, respectively) are regulated by the FNR-type proteins FnrP, NarR, and NNR. FnrP contains a 4Fe-4S cluster for sensing O_2, and NNR harbours a NO-sensing haem; NarR, however, is poorly characterised and is most likely a NO_2^--sensor [19–21]. All these sensors remain inactive during aerobic growth conditions [19].

Transcription of denitrification genes in *Pa. denitrificans*. FnrP and NarR facilitate a product-induced transcription of the *nar* genes, and NNR facilitates a product-induced transcription of the *nirS* genes (Fig 1, see P_1 and P_2): Low oxygen concentration ($[O_2]$) activates the self-regulating FnrP, which induces *nar* transcription in coaction with NarR. The self-regulating NarR was previously assumed to be activated by either NO_3^- or NO_2^- [21], but a recent proteomics study indicates that NO_2^- is the activator [19]. Thus once a cell starts producing traces of NO_2^-, *nar* expression becomes autocatalytic. Transcription of *nirS* is induced by NNR, which is apparently inactivated by O_2 [22,23], but under anoxic/micro-oxic conditions, NNR is activated by NO. Thus, once traces of NO are produced, the expression of *nirS* also becomes

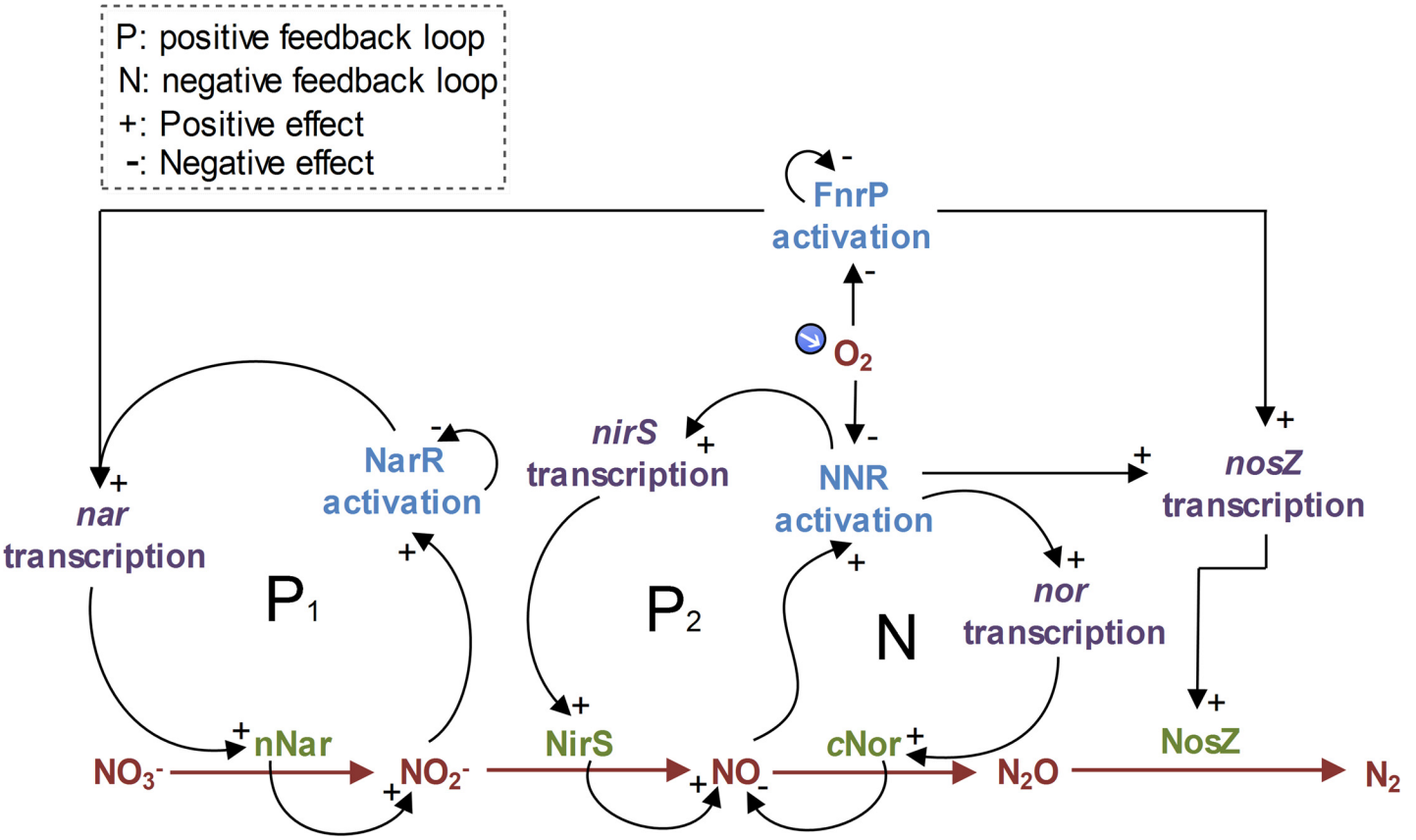

Fig 1. Regulatory network of denitrification in *Pa. denitrificans*. The network is driven by four core enzyme-complexes: Nar (transmembrane nitrate reductase encoded by the *narG* gene), NirS (cytochrome cd_1 nitrite reductase encoded by *nirS*), cNor (NO reductase encoded by *norBC*), and NosZ (N_2O reductase encoded by *nosZ*). When anoxia is imminent, the low [O_2] is sensed by FnrP, which in some interplay with NarR induces *nar* transcription. NarR is activated by NO_2^-; thus once a cell starts producing traces of NO_2^-, *nar* expression becomes autocatalytic (see P_1). Transcription of *nirS* is induced by NNR, which is activated under anoxic/micro-oxic conditions by NO; thus once traces of NO are produced, the expression of *nirS* also becomes autocatalytic (see P_2) [20]. The activated P_2 will also induce *nor* and *nosZ* transcription via NNR. The transcription of *nosZ*, however, can also be induced equally and independently by FnrP [24]. Micromolar concentrations of NO may inactivate both FnrP [25] and NosZ [26]. These observations, however, are ignored for our modelling because *Pa. denitrificans* restricts NO to nanomolar levels.

doi:10.1371/journal.pcbi.1004621.g001

autocatalytic [19,20]. In contrast, *nor* transcription is substrate (NO) induced via NNR while *nosZ* is equally induced by NNR or FnrP [24]. High concentrations of NO may constrain *nar* transcription by inactivating FnrP [25] and, like O_2, render NosZ dysfunctional by inactivating the Cu_Z subunit of the reductase [26], but these observations are ignored in our model because *Pa. denitrificans* restricts [NO] to very low levels.

Entrapment of cells in anoxia: The underlying hypothesis and modelling

Denitrification proteome, once produced in response to an anoxic spell, is likely to linger within the cells under subsequent oxic conditions, ready to be used if anoxia recurs. But the proteome will be diluted by aerobic growth because the transcription of denitrification genes is inactivated under oxic conditions [20]. Hence, a population growing through many generations under fully oxic conditions is expected to undertake *de novo* synthesis of denitrification enzymes when confronted with anoxia. Batch cultivations of such aerobically raised *Pa. denitrificans* provided indirect evidence for a novel claim that, in response to anoxia, only a small fraction of the incubated population is able to produce denitrification proteome [8,17,27,28]. Our dynamic modelling of

Bergaust *et al.'s* [17] NO_2^--supplemented incubations corroborated this, suggesting that a probabilistic function (specific probability = 0.005 h^{-1}) resulting in the recruitment of 3.8–16.1% of all cells to denitrification is adequate to explain the measured N_2 kinetics [16].

Our model was based on the hypothesis that the entrapment of a large fraction in anoxia is due to a low probability of initiating *nirS* transcription, which in response to O_2 depletion is possibly mediated through a minute pool of intact NNR, crosstalk with other factors (such as FnrP), unspecific reduction of NO_2^- to NO by Nar, and/or through non-biologically formed traces of NO found in a NO_2^--supplemented medium. Regardless of the exact mechanism(s), once *nirS* transcription is initiated, the positive feedback via NO/NNR (Fig 1, see P_2) would allow the product of a single transcript of *nirS* to induce a subsequent burst of *nirS* transcription. The activated positive feedback will also help induce *nor* and *nosZ* transcription via NNR, rapidly transforming a cell into a full-fledged denitrifier. We further hypothesised that recruitment to denitrification will only be possible as long as a minimum of O_2 is available because, since *Pa. denitrificans* is non-fermentative, the synthesis of first molecules of NirS will depend on energy from aerobic respiration.

The above hypothesis was modelled by segregating the culture into two pools (subpopulations): one for the cells without (N_{D-}) and the other with denitrification enzymes (N_{D+}). Initially, all cells were N_{D-}, growing by consuming O_2. As [O_2] fell below a certain threshold, N_{D-} recruited to N_{D+} with a constant probability (h^{-1}), assumed to be that of the *nirS* transcriptional activation, and the recruitment halted as O_2 was completely exhausted, assuming lack of energy (ATP) for enzyme synthesis.

Underlying assumptions and aims of the present modelling

The present model is an extension of that developed in Hassan *et al.* [16]. Here we have divided the respiring culture into four pools (Fig 2A):

1. Z^-: cells without Nar, NirS, and *c*Nor
2. Z^{Na}: cells with Nar
3. Z^{NaNi}: cells with Nar, NirS, and *c*Nor
4. Z^{Ni}: cells with NirS and *c*Nor

All these subpopulations are assumed to scavenge O_2 (if present) and produce NosZ in response to impending anoxia. The latter because the *nosZ* genes are readily induced by the O_2-sensor FnrP [24].

The Z^- pool (Fig 2A) contains the inoculum that grows by aerobic respiration. As [O_2] falls below a critical threshold [empirically determined, 18], the cells within Z^- are assumed to start synthesising Nar with a certain probability and populate the Z^{Na} pool. The aim here is to investigate whether, like for *nirS*, the initiation of *nar* transcription (by some combined activity of FnrP and NarR) can also be explained as a probabilistic phenomenon, quickly differentiating a cell into a full-fledge NO_3^- scavenger through product (NO_2^-) induced transcription via NarR (Fig 1, see P_1). If so, we were interested to estimate what fraction of the cells is required to adequately simulate the measured data (NO_2^- production), aiming at scrutinising the general assumption that all cells in batch cultures produce Nar in response to impending anoxia.

Next, when [O_2] is further depleted to another critical threshold [18], the Z^- and Z^{Na} cells are assumed to initiate *nirS* transcription with a low per hour probability and, thereby, populate the Z^{Ni} and Z^{NaNi} pools, respectively. As explained above for our previous model, NirS + *c*Nor production is assumed to be *a)* coordinated because the transcription of both *nirS* and *nor* is induced by NO via the NO-sensor NNR (Fig 1), and *b)* stochastic because the initial transcription of *nirS*

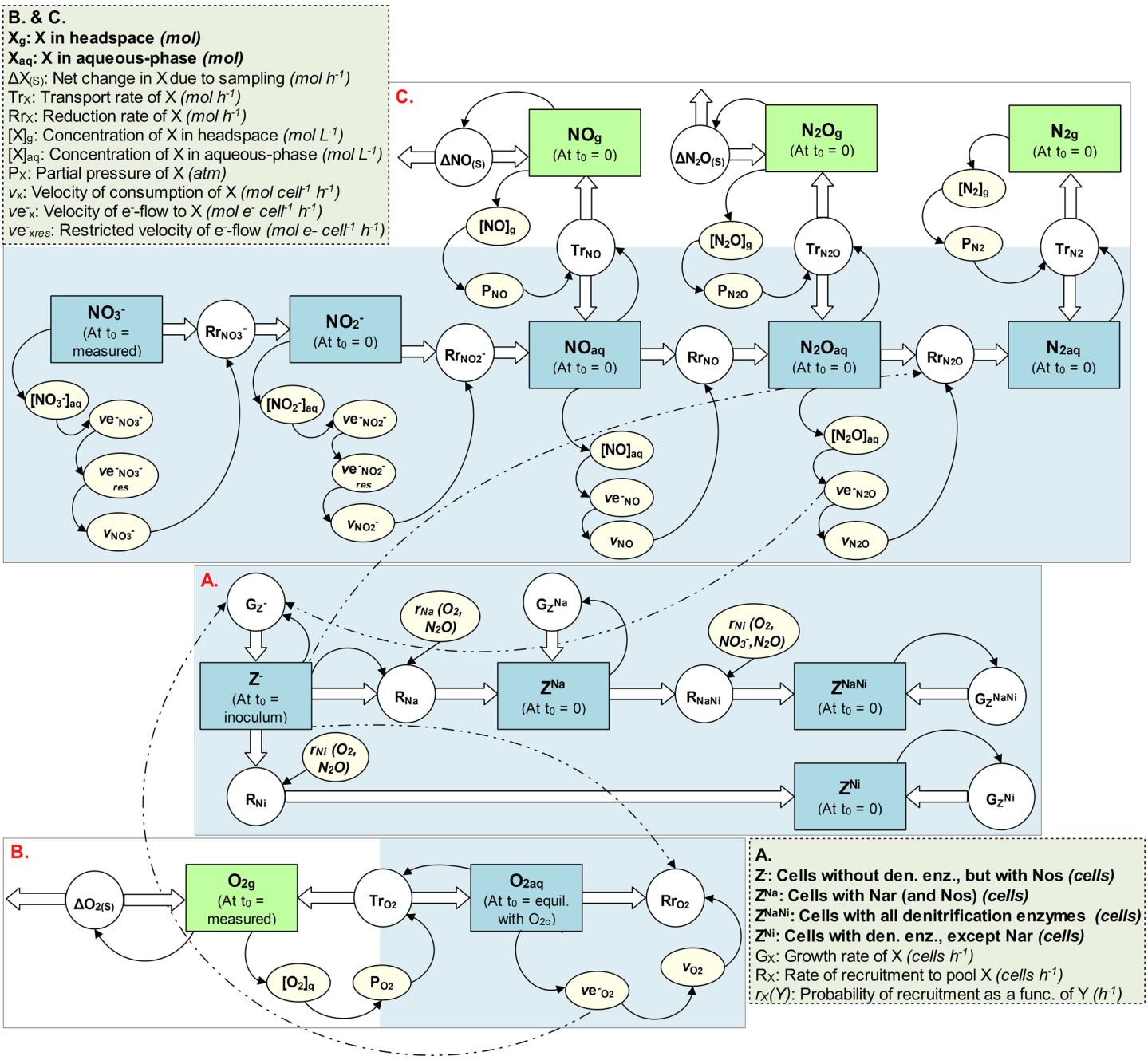

Fig 2. A stock and flow diagram illustrating the model's structure. A. Cell diversification and growth; **B.** O_2 kinetics; **C.** Denitrification kinetics. The squares represent state variables, the circles the rate of change of the state variables, the edges (thicker arrows) depict flows into or out of the state variables, the shaded ovals auxiliary variables, and the arrows portray mutual dependencies between the variables. All feedback relationships among the three model sectors could not be shown; however, for illustration the feedback relationships of one sub-population (Z^-) are shown (dashed arrows). Within each square (state variable), t_0 refers to the initial value.

doi:10.1371/journal.pcbi.1004621.g002

(paving the way for the autocatalytic expression of NirS and substrate-induced *nor* transcription) happens in the absence of NO or at too low [NO] to be sensed by NNR.

Synthesis of denitrification enzymes requires energy, which all the subpopulations can obtain by respiration only. Hence, the initiation of the autocatalytic expression of *nar* and *nirS*

(i.e., recruitment to Z^{Na} and Z^{NaNi}/Z^{Ni}, respectively, Fig 2A) depends on the availability of the relevant terminal e^--acceptor(s) above a critical concentration to sustain a minimum of respiration. For Z^-, the only relevant e^--acceptors are O_2 and the traces of N_2O produced by Z^{Ni} and Z^{NaNi}. The same applies For Z^{Na}, but in addition, this subpopulation can also obtain energy by reducing NO_3^-, if present. In our previous model [16], we assumed that recruitment to denitrification was sustained by energy from O_2-respiration only; not NO_3^- because we simulated NO_2^--supplemented treatments, and not by N_2O because we naively assumed that the pool of this e^--acceptor was insignificant (N_2O concentrations were below the detection limit of the system used for those experiments). However, the present model assumes that the recruitment from Z^- to Z^{Na} and Z^- to Z^{Ni} is sustained by both O_2- and N_2O-reduction, and the recruitment from Z^{Na} to Z^{NaNi} is sustained by O_2-, N_2O- and NO_3^--reduction, when above a critical minimum (ve^-_{min}). The default value for ve^-_{min} was set to an arbitrary low value (= 0.44% of the maximum e^--flow rate to O_2), and we have investigated the consequences of increasing, decreasing, and setting $ve^-_{min} = 0$.

The expressions of *nar* and *nirS* + *nor* (recruitments to Z^{Na} and Z^{NaNi}/Z^{Ni}, respectively, Fig 2A) are modelled as instantaneous discrete-events in each cell, thus ignoring the time-lag from the initiation of gene transcription till the cell is fully equipped with the reductase(s) in question. That is because the lag observed between the emergence of denitrification gene transcripts and the subsequent gas products suggests that the synthesis of denitrification enzymes takes less than half an hour [17,18], which is negligible for our purposes here.

The main purpose of the present modelling is to investigate if a full-fledged model, including all four functional denitrification reductases, could adequately simulate the observed kinetics and stoichiometry of denitrification products [18]. These cultures reduced all available NO_3^- to NO_2^- prior to the onset of gas production and accumulated traces of N_2O throughout the anoxic phase, as illustrated in S1 Fig In particular, we were interested to investigate the NO_2^- kinetics, controlled by *nar*- and *nirS* transcription, and to test if the peculiar N_2O kinetics (low, but increasing concentrations throughout the anoxic phase) could be explained by our modelled cell diversification.

Materials and Methods

An overview of the modelled experiment

Batch incubation. Qu [18] incubated *Pa. denitrificans* (DSM-413) at 20°C using 50 mL Sistrom's [29] medium in 120 mL gas-tight vials. Either succinate or butyrate (5 mM) was used as the main carbon source, enough to secure consumption of all available e^--acceptors. After distribution of the medium, each vial was loaded with a magnetic stirring bar, sterilised through autoclaving, supplemented with 2 mM KNO_3, and was tightly sealed. To remove O_2 and N_2 from the headspace, the headspace air was evacuated and replaced by helium (He) through several cycles of evacuation and He-filling (He-washing). Some vials were supplemented with oxygen to reach 7 vol.% O_2 in headspace (treatment designated 7% O_2). The remaining vials received no O_2 (designated 0% O_2, although there were traces of O_2 present despite the He washing). For each treatment (i.e., C source and initial O_2), there were three replicates, and each vial was inoculated with 2.2×10^8 aerobically grown cells.

NO_2^- and gas measurement. Gases (CO_2, O_2, NO, N_2O, and N_2) were monitored by frequent sampling of the headspace, using an improved version of the robotised incubation system [30]. In short, the system draws gas samples from the headspace (peristaltic pumping) via the septum pierced by a needle, filling three loops used for injecting samples into the two GC columns and the chemiluminescence NO analyser. The sample drawn is replaced by He (reversing the peristaltic pump), thus securing ~1 atm pressure. The primary improvements of the new system are a more sensitive detection of N_2O (by an electron capture detector), lower

sampling volumes (~1 mL), and lower leaks of O_2 and N_2 through the sampling system (4 nmol O_2 and 12 nmol N_2 per sampling, which is ~20% of that for the old system).

To extract samples for measuring NO_2^- without tampering the original vials, identical (parallel) vials were prepared for each treatment. Using sterile syringes, samples of 0.1 mL were regularly drawn from the liquid-phase of the parallel vials and immediately analysed for NO_2^-.

Results for one of the treatments are shown in S1 Fig, illustrating the complete reduction of NO_3^- to NO_2^- prior to the onset of significant N-gas production. In previous experiments [17], N_2O concentrations were below the detection limit of the system, but thanks to the new system, the N_2O kinetics were monitored with a reasonable precision.

The model

The model is constructed in Vensim DSS 6.2 Double Precision (Ventana Systems, inc. http://vensim.com/) using techniques from the field of system dynamics [31].

Cell diversification and growth. The respiring population is divided into four subpopulations, according to their reductases (Fig 2A): 1) Z^-: cells without Nar, NirS, and *c*Nor; 2) Z^{Na}: cells with Nar; 3) Z^{NaNi}: cells with Nar, NirS, and *c*Nor; and 4) Z^{Ni}: cells with NirS and *c*Nor. All the subpopulations are assumed to equally respire O_2, if present, and express *nosZ* in response to oxygen depletion [24]. Z^- contains the inoculum (= 2.2×10^8 cells) that grows by aerobic respiration. As O_2 is depleted, the Z^- cells populate the other pools by producing Nar and/or NirS + *c*Nor.

The recruitment from Z^- to Z^{Na} (R_{Na}, Fig 2A) takes place first:

$$R_{Na} = Z^- \times r_{Na}(O_2, N_2O) \quad (1)$$

(cells h^{-1})

where $r_{Na}(O_2,N_2O)$ is a conditional specific probability (h^{-1}) for any Z^- cell to initiate *nar* transcription (quickly transforming it into a NO_3^- scavenger through autocatalytic gene expression, see Fig 1, P_1):

$$\begin{aligned} & r_{Na}(O_2, N_2O) = \\ & \textbf{IF} \quad [O_2]_{aq} < [O_2]_{na} \ \textbf{AND} \ (ve^-_{O_2} + 0.5 \times ve^-_{N_2O}) > ve^-_{min} \\ & \textbf{THEN} \quad r_{Na} \\ & \textbf{ELSE} \quad 0 \end{aligned} \quad (2)$$

(h^{-1})

where r_{Na} (h^{-1}) is a constant specific probability for a cell to initiate *nar* transcription once O_2 concentration in the aqueous-phase ($[O_2]_{aq}$, mol L^{-1}) falls below a critical concentration ($[O_2]_{na}$), empirically determined as the $[O_2]_{aq}$ (= 4.75×10^{-5} mol L^{-1}) at the outset of NO_2^- accumulation in the medium [18]. The second condition for a cell to produce first molecules of Nar is a minimum of e^--flow to an e^--acceptor (ve^-_{min}, mol e^- $cell^{-1}$ h^{-1}), assumed to generate minimum ATP required for protein synthesis. $ve^-_{O_2}$ and $ve^-_{N_2O}$ (mol e^- $cell^{-1}$ h^{-1}) are the cell-specific velocities of e^--flow to O_2 and N_2O, respectively. The latter is weighed down by 0.5 because mole ATP per mole e^- transferred to NO_x^-/NO_x is lower for denitrification than for aerobic respiration [17,20]. For a Z^- cell, $ve^-_{NO_2^-}$ and ve^-_{NO} are not considered here, since such a cell is assumed to have no NirS and *c*Nor.

The fraction of the cells that successfully produces Nar (F_{Na}) is calculated based on the integral of the recruitment (Eq 1):

$$F_{Na} = 1 - e^{-r_{Na} \times t_{Na}} \quad (3)$$

(dimensionless)

where t_{Na} is the time-window available for the recruitment. In theory, t_{Na} is the time-period when $[O_2]_{aq} < [O_2]_{na}$ **AND** $(ve^-_{O_2} + 0.5 \times ve^-_{N_2O}) > ve^-_{min}$ (Eq 2). Since the e^--flow to N_2O started after all NO_3^- had been reduced to NO_2^- (S1 Fig), the recruitment based on $ve^-_{N_2O}$ would be inconsequential for the simulated (and measured) NO_2^- kinetics. Therefore, to calculate the functional F_{Na} actually responsible for producing NO_2^-, we ignored the N_2O-sustained recruitment, thus considering t_{Na} to be the time when $[O_2]_{aq} < [O_2]_{na}$ **AND** $ve^-_{O_2} > ve^-_{min}$.

Next, the cells within Z^{Na} and Z^- are recruited to Z^{NaNi} and Z^{Ni} (R_{NaNi} and R_{Ni}, respectively, Fig 2A), as they are assumed to stochastically initiate *nirS* transcription, paving the way for NO/NNR mediated autocatalytic expression of *nirS* + *nor* (Fig 1). In principle, the rates of both these recruitments are modelled as that of the recruitment from Z^- to Z^{Na} (Eqs 1 and 2): *a)* Both trigger as O_2 falls below another critical concentration ($[O_2]_{ni}$), low enough to activate NNR to induce *nirS* transcription; $[O_2]_{ni}$ (= 1.16×10^{-5} mol L^{-1}) is empirically determined as the O_2 concentration at the outset of NO accumulation [18]. *b)* Both continue as long as a minimum of e^--flow to the relevant terminal e^--acceptor is possible, sustaining the respiratory metabolism to generate ATP for protein synthesis:

$$R_{NaNi} = Z^{Na} \times r_{Ni}(O_2, NO_3^-, N_2O) \tag{4}$$

(cells h^{-1})

$$\begin{aligned} &r_{Ni}(O_2, NO_3^-, N_2O) = \\ &\textbf{IF} \quad [O_2]_{aq} < [O_2]_{ni} \textbf{ AND } (ve^-_{O_2} + 0.5 \times ve^-_{NO_3^-} + 0.5 \times ve^-_{N_2O}) > ve^-_{min} \\ &\textbf{THEN} \quad r_{Ni} \\ &\textbf{ELSE} \quad 0 \end{aligned} \tag{5}$$

(h^{-1})

where r_{Ni} is a constant specific probability (h^{-1}) for the initiation of *nirS* transcription. $ve^-_{NO_3^-}$ and $ve^-_{N_2O}$ are multiplied with 0.5 for the same reasons as described for Eq 2.

The recruitment from Z^- to Z^{Ni} (R_{Ni}, Fig 2A) is modelled as a product of Z^- and a conditional specific probability, $r_{Ni}(O_2,N_2O)$, which is different from Eq 5 only in that $ve^-_{NO_3^-}$ is omitted, since Z^- do not possess Nar:

$$R_{Ni} = Z^- \times r_{Ni}(O_2, N_2O) \tag{6}$$

(cells h^{-1})

$$\begin{aligned} &r_{Ni}(O_2, N_2O) = \\ &\textbf{IF} \quad [O_2]_{aq} < [O_2]_{ni} \textbf{ AND } (ve^-_{O_2} + 0.5 \times ve^-_{N_2O}) > ve^-_{min} \\ &\textbf{THEN} \quad r_{Ni} \\ &\textbf{ELSE} \quad 0 \end{aligned} \tag{7}$$

(h^{-1})

The fraction that successfully produced NirS + *c*Nor (F_{Ni}) is calculated based on the integral of R_{NaNi} and R_{Ni}:

$$F_{Ni} = (1 - e^{-r_{Ni} \times t_{NaNi}}) \times F_{Na} + (1 - e^{-r_{Ni} \times t_{Ni}}) \times (1 - F_{Na}) \tag{8}$$

(dimensionless)

where t_{NaNi} is the duration of the recruitment from Z^{Na} to Z^{NaNi}, i.e., when $[O_2]_{aq} < [O_2]_{ni}$ **AND** $(ve^-_{O_2} + 0.5 \times ve^-_{NO_3^-} + 0.5 \times ve^-_{N_2O}) > ve^-_{min}$ (Eqs 4 and 5), F_{Na} is the fraction recruited to the pool of Nar positive cells (Z^{Na}, Eq 3), and t_{Ni} is the duration of the recruitment from Z^- to Z^{Ni}, i.e., when $[O_2]_{aq} < [O_2]_{ni}$ **AND** $(ve^-_{O_2} + 0.5 \times ve^-_{N_2O}) > ve^-_{min}$ (Eqs 6 and 7).

Each of the populations will grow depending on the rates of e^--flow to the various e^--acceptors they are able to use:

$$G_{Z^-} = Z^- \times (Ye^-_{O_2} \times ve^-_{O_2} + Ye^-_{NO_x} \times ve^-_{N_2O}) \quad (9)$$

$$G_{Z^{Na}} = Z^{Na} \times [Ye^-_{O_2} \times ve^-_{O_2} + Ye^-_{NO_x} (ve^-_{NO_3^- res} + ve^-_{N_2O})] \quad (10)$$

$$G_{Z^{NaNi}} = Z^{NaNi} \times [Ye^-_{O_2} \times ve^-_{O_2} + Ye^-_{NO_x} (ve^-_{NO_3^- res} + ve^-_{NO_2^- res} + ve^-_{NO} + ve^-_{N_2O})] \quad (11)$$

$$G_{Z^{Ni}} = Z^{Ni} \times [Ye^-_{O_2} \times ve^-_{O_2} + Ye^-_{NO_x} (ve^-_{NO_2^- res} + ve^-_{NO} + ve^-_{N_2O})] \quad (12)$$

(cells h^{-1})

where Ye^-_X (cells mol^{-1} e^- to X = O_2 or NO_x^-/NO_x) is the growth yield determined under the actual experimental conditions, and ve^-_X (mol e^- $cell^{-1}$ h^{-1}) is the cell-specific velocity of e^--flow to X (O_2 or NO_x^-/NO_x), which depends on the concentration of the e^--acceptor (see Eqs 17, 20 and 28). For NO_3^- and NO_2^-, a restricted velocity ($ve^-_{NO_x^- res}$) is used so that when electrons flow to O_2, NO_3^-, and NO_2^- simultaneously, the total ve^- per cell does not exceed the maximum electrons that the TCA cycle ($ve^-_{max\mathrm{TCA}}$) can deliver per hour (see Eqs 21 and 22).

O_2 kinetics. O_2 is initially present in the headspace (O_{2_g}, mol, initialised according to the experiment, see Table 1) but is transported to the liquid-phase ($O_{2_{aq}}$) due to its consumption therein (Fig 2B). The transport rate (Tr_{O_2}) is modelled according to Molstad *et al.* [30]:

$$Tr_{O_2} = k_t (k_{H(O_2)} \times P_{O_2} - [O_2]_{LP}) \quad (13)$$

(mol h^{-1})

where k_t (L h^{-1}) is the empirically determined coefficient for the transport of gas between the headspace and the liquid, $k_{H(O_2)}$ (mol L^{-1} atm^{-1}) is the solubility of O_2 in water at 20°C, P_{O_2} (= $[O_2]_g \times R \times T$, atm) is the partial pressure of O_2 in the headspace, and $[O_2]_{aq}$ (mol L^{-1}) is the O_2 concentration in the liquid $\left([O_2]_{aq} = \frac{O_{2_{aq}}}{Vol_{aq}}\right)$.

In addition, the model simulates the changes in O_{2_g} due to sampling. The robotised incubation system used monitors gas concentrations by sampling the headspace, where each sampling alters the concentrations in a predictable manner: a fraction of O_{2_g} is removed and replaced by

Table 1. Simulated experiment [18].

Batch	C-source	$O_{2_g}(t_0)$ (vol.%)*	$NO_3^-(t_0)$ (mM)	Replicates
1	Butyrate	~0	2	3
2	Butyrate	7	2	3
3	Succinate	~0	2	3
4	Succinate	7	2	3

*Target values for initial O_2 concentrations in the headspace (vol.%). ~0 means that the intended concentration should be zero, but there were detectable traces of O_2, despite several cycles of evacuation and He-flushing of the headspace.

doi:10.1371/journal.pcbi.1004621.t001

He (dilution), but the sampling also results in a marginal leakage of O_2 through the tubing and membranes in the injection system. The net change in O_{2_g} ($\Delta O_{2(S)}$) as a result of each sampling is calculated as:

$$\Delta O_{2(S)} = \frac{O_{2_{leak}} - O_{2_g} \times D}{t_s} \quad (14)$$

(mol h^{-1})

where $O_{2_{leak}}$ (mol $vial^{-1}$) is the O_2-leakage into the headspace, D (dilution) is the fraction of each headspace gas removed and replaced by equal amount of He, and t_s (h) is the time taken to complete each sampling. $\Delta O_{2(S)}$ is negative if O_{2_g} is high and marginally positive at very low oxygen concentrations.

O_2 in the liquid-phase ($O_{2_{aq}}$, mol, Fig 2B) is initialised by assuming equilibrium with O_{2_g} at the time of inoculation ($O_{2_{aq}}(t_0) = P_{O_2} \times k_{H(O_2)} \times Vol_{aq}$). The dynamics of $O_{2_{aq}}$ are modelled as a function of transport between the headspace and the liquid (Tr_{O_2}, Eq 13) and its reduction rate (Rr_{O_2}, mol h^{-1}):

$$\frac{d(O_{2_{aq}})}{dt} = Tr_{O_2} - Rr_{O_2} \quad (15)$$

$$Rr_{O_2} = (Z^{-} + Z^{Na} + Z^{NaNi} + Z^{Ni}) \times \nu_{O_2} \quad (16)$$

(mol h^{-1})

where Z^{-}, Z^{Na}, Z^{NaNi}, and Z^{Ni} (cells) are all the sub-populations present (described above); thus, we assume that all cells have the same potential to consume O_2. ν_{O_2} (mol $cell^{-1}$ h^{-1}) is the cell-specific velocity of O_2 consumption, obtained by the velocity of e^--flow to O_2 $\left(\nu e^-_{O_2}, \frac{1 \text{ mol}O_2}{4 \text{ mol } e^-}\right)$, where $\nu e^-_{O_2}$ is modelled as a Michaelis-Menten function of oxygen concentration:

$$\nu e^-_{O_2} = \frac{\nu e^-_{max O_2} \times [O_2]_{aq}}{K_{mO_2} + [O_2]_{aq}} \quad (17)$$

(mol e^- $cell^{-1}$ h^{-1})

where $\nu e^-_{max O_2}$ (mol e^- $cell^{-1}$ h^{-1}) is the maximum velocity of e^--flow to O_2 per cell (determined under the actual experimental conditions), $[O_2]_{aq}$ (mol L^{-1}) is the O_2 concentration in the liquid-phase, and K_{mO_2} (mol L^{-1}) is the half-saturation constant for O_2 reduction.

Denitrification kinetics. The NO_3^- and NO_2^- pools (mol, Fig 2C) are initialised according to the experiment (Table 1; $NO_2^- = 0$). The kinetics of these nitrogen oxyanions (NO_x^-) are modelled as:

$$\frac{d(NO_3^-)}{dt} = -Rr_{NO_3^-} = -(Z^{Na} + Z^{NaNi}) \times \nu_{NO_3^-} \quad (18)$$

$$\frac{d(NO_2^-)}{dt} = Rr_{NO_3^-} - Rr_{NO_2^-} = Rr_{NO_3^-} - (Z^{NaNi} + Z^{Ni}) \times \nu_{NO_2^-} \quad (19)$$

(mol h^{-1})

where $Rr_{NO_x^-}$ (mol h^{-1}) is the reduction rate, $Z^{Na} + Z^{NaNi}$ (cells) is the total number of cells with Nar, $Z^{NaNi} + Z^{Ni}$ (cells) is the total NirS active population, and $\nu_{NO_x^-}$ (mol $cell^{-1}$ h^{-1}) is the

cell-specific velocity of NO_x^- consumption, obtained by the velocity of e^--flow to NO_x^- $\left(\frac{1 \text{ mol } NO_3^-}{2 \text{ mol } e^-} \text{ and } \frac{1 \text{ mol } NO_2^-}{1 \text{ mol } e^-}\right)$. The latter is modelled as a Michaelis-Menten function of NO_x^- concentration:

$$ve^-_{NO_x^-} = \frac{ve^-_{maxNO_x^-} \times [NO_x^-]_{aq}}{K_{mNO_x^-} + [NO_x^-]_{aq}} \quad (20)$$

(mol e^- $cell^{-1}$ h^{-1})

where $ve^-_{maxNO_x^-}$ (mol e^- $cell^{-1}$ h^{-1}) is the maximum velocity of e^--flow to NO_x^- per cell (determined under the actual experimental conditions), $[NO_x^-]_{aq}$ (mol L^{-1}) is the NO_x^- concentration in the aqueous-phase, and $K_{mNO_x^-}$ (mol L^{-1}) is the half-saturation constant for NO_x^- reduction.

The velocity of NO_3^- and NO_2^- consumption had to be restricted ($ve^-_{NO_x^- res}$) to ensure that when electrons flow to O_2, NO_3^-, and NO_2^- simultaneously, the total ve^- per cell does not exceed an estimated maximum delivery of electrons from the TCA cycle (ve^-_{maxTCA}). In competition for electrons, O_2 is prioritised [20], followed by NO_3^- and NO_2^-, respectively [18]:

$$ve^-_{NO_3^- res} = \text{Min}\,(ve^-_{NO_3^-}, (ve^-_{maxTCA} - ve^-_{O_2})) \quad (21)$$

$$ve^-_{NO_2^- res} = \text{Min}\,(ve^-_{NO_2^-}, (ve^-_{maxTCA} - ve^-_{O_2} - ve^-_{NO_3^- res})) \quad (22)$$

(mol e^- $cell^{-1}$ h^{-1})

where $ve^-_{NO_3^- res}$ is the realised e^--flow to NO_3^-, limited either by available NO_3^- or the availability of electrons (due to competition with O_2); $ve^-_{NO_2^- res}$is the realised e^--flow to NO_2^-. Such competition for electrons was not implemented for ve^-_{NO} and $ve^-_{N_2O}$ because at the onset of NO-, N_2O- and N_2 production, the total velocity of e^--flow to all available e^--acceptors (as predicted by the enzyme kinetics alone) never exceeded ve^-_{maxTCA}.

Gas consumption and production takes place in the aqueous phase, but the gases are transported between aqua and the headspace depending on their concentrations in the two phases. Each gas in aqua, X_{aq} (molN, Fig 2C), is modelled as a function of production, consumption (not applicable to N_2), and the net transport, where N_2O_{aq} and $N_{2_{aq}}$ are initialised with zero, and NO_{aq} is initialised with a negligible 1×10^{-25} mol to avoid division by zero (in Eq 28).

$$\frac{d(NO_{aq})}{dt} = Rr_{NO_2^-} - Rr_{NO} + Tr_{NO} \quad (23)$$

$$\frac{d(N_2O_{aq})}{dt} = Rr_{NO} - Rr_{N_2O} + Tr_{N_2O} \quad (24)$$

$$\frac{d(N_{2_{aq}})}{dt} = Rr_{N_2O} + Tr_{N_2} \quad (25)$$

(molN h^{-1})

where Rr_{NO_x} (molN h^{-1}) is the relevant NO_x^-/NO_x reduction rate, and Tr_{N_X} represents the gas transport rate between aqua and the headspace (Eq 29; N.B. $Tr_{N_X} < 0$ for the net transport from aqua to the headspace).

The reduction of NO to N_2O (Rr_{NO}) and N_2O to N_2 (Rr_{N_2O}) is modelled likewise as a function of the number of relevant cells and the velocity of e^--flow to NO and N_2O (mol e^- $cell^{-1}$ h^{-1}),

respectively:

$$\mathrm{Rr_{NO}} = (\mathrm{Z^{NaNi}} + \mathrm{Z^{Ni}}) \times \nu_{\mathrm{NO}} \tag{26}$$

$$\mathrm{Rr_{N_2O}} = (\mathrm{Z^{-}} + \mathrm{Z^{Na}} + \mathrm{Z^{NaNi}} + \mathrm{Z^{Ni}}) \times \nu_{\mathrm{N_2O}} \tag{27}$$

$(\mathrm{molN\ h^{-1}})$

where ν_{NO} and $\nu_{\mathrm{N_2O}}$ are obtained by the velocity of e^--flow to NO and N_2O, respectively $\left(1\,\frac{\mathrm{mol\ N}}{\mathrm{mol\ e^-}}\right)$. $\nu e^-_{\mathrm{N_2O}}$ is modelled as a Michaelis-Menten function of $[N_2O]_{aq}$, similarly as that of O_2, NO_3^-, and NO_2^- (Eqs 17 and 20), but νe^-_{NO} is modelled assuming a cooperative binding of two NO molecules with *c*Nor to form N_2O [32]:

$$\nu e^-_{\mathrm{NO}} = \frac{\nu e^-_{max\mathrm{NO}}}{1 + \mathrm{K_{2NO}}\left(\frac{1}{[\mathrm{NO}]_{aq}} + \frac{\mathrm{K_{1NO}}}{[\mathrm{NO}]_{aq}^2}\right)} \tag{28}$$

$(\mathrm{mol\ cell^{-1}\ h^{-1}})$

where $\nu e^-_{max\mathrm{NO}}$ $(\mathrm{mol\ e^-\ cell^{-1}\ h^{-1}})$ is the empirically determined maximum velocity of e^--flow to NO per cell, $[\mathrm{NO}]_{aq}$ $(\mathrm{mol\ L^{-1}})$ is the NO concentration in the liquid-phase, and $\mathrm{K_{1NO}}$ & $\mathrm{K_{2NO}}$ $(\mathrm{mol\ L^{-1}})$ are the equilibrium dissociation constants for the *c*Nor/NO- and *c*Nor/$(NO)_2$ complex, respectively.

The transport of NO, N_2O, and N_2between the liquid and the headspace (Eqs 23–25) is modelled as:

$$\mathrm{Tr_N} = \mathrm{k_t} \times (\mathrm{k_{H(N)}} \times \mathrm{P_N} - [\mathrm{N}]_{aq}) \tag{29}$$

$(\mathrm{molN\ h^{-1}})$

where k_t is the empirically determined coefficient for the transport of each gas between the headspace and the liquid, $k_{H(N)}$ $(\mathrm{molN\ L^{-1}\ atm^{-1}})$ is the solubility of NO, N_2O, or N_2 in water at 20°C, P_N (= $[N]_g \times R \times T$, atm) is the partial pressure of each gas in the headspace, and $[N]_{aq}$ $(\mathrm{mol\ L^{-1}})$ represents the concentration of each gas in the liquid-phase.

The amount of NO and N_2O in the headspace (NO_{x_g}, molN, Fig 2C) is a function of transport (Eq 29) and the disturbance by gas sampling. The latter is simulated as discrete events at time-points given as input to the model (equivalent to the sampling times in the experiment):

$$\Delta\mathrm{NO_{x(S)}} = \frac{\mathrm{NO_{x_g}} \times \mathrm{D}}{\mathrm{t_s}} \tag{30}$$

$(\mathrm{molN\ h^{-1}})$

where $\Delta NO_{x(S)}$ is the net change in the amount of NO_{x_g} (molN), D (dilution) is the fraction of each gas removed and replaced by equal amount of He, and t_s (h) is the time taken to complete each sampling. For N_2, the model ignores the sampling loss because the N_2 production data to be compared with the model output are already corrected for the sampling disturbance [30]. Thus, the model estimates somewhat higher N_2 concentrations than that experienced by the organisms, which is acceptable, since the concentration of N_2 is unlikely to have consequences for the metabolism.

Parameterisation

Most of the parameter values used in the model are well established in the literature (see Table 2); however, uncertain parameters include $\mathrm{K}_{m\mathrm{O}_2}$, $\mathrm{K}_{m\mathrm{N}_2\mathrm{O}}$, $\nu e^-_{max\mathrm{O}_2}$, and νe^-_{min}.

Table 2. Model parameters.

	Description	Value	Units	Reference
Butyrate treatments				
ve^-_{maxTCA}	Max. cell-specific rate of e^--delivery from the TCA cycle	1×10^{14}	mol e^- $cell^{-1}$ h^{-1}	[18]
$ve^-_{maxO_2}$	The maximum cell-specific velocity of e^--flow to O_2	4.22×10^{-15}	mol e^- $cell^{-1}$ h^{-1}	Optimisation
$ve^-_{maxNO_3^-}$	The maximum cell-specific velocity of e^--flow to NO_3^-	1×10^{-14}	mol e^- $cell^{-1}$ h^{-1}	[18]
$ve^-_{maxNO_2^-}$	The maximum cell-specific velocity of e^--flow to NO_2^-	2.65×10^{-15}	mol e^- $cell^{-1}$ h^{-1}	[18]
ve^-_{min}	The min. velocity of e^--flow to O_2/NO_x^-/NO_x required for protein synthesis (ATP)	1.87×10^{-17}	mol e^- $cell^{-1}$ h^{-1}	Assumption
$Ye^-_{O_2}$	The growth yield per mole of electrons transferred to O_2	2.74×10^{13}	cells (mol e^-)$^{-1}$	[18]
$Ye^-_{NO_x}$	The growth yield per mole e^- to NO_3^-, NO_2^-, NO, or N_2O	1.12×10^{13}	cells (mol e^-)$^{-1}$	[18]
Succinate treatments				
ve^-_{maxTCA}	Max. cell-specific rate of e^--delivery from the TCA cycle	9.34×10^{-15}	mol e^- $cell^{-1}$ h^{-1}	[18]
$ve^-_{maxO_2}$	The maximum cell-specific velocity of e^--flow to O_2	4.42×10^{-15}	mol e^- $cell^{-1}$ h^{-1}	[18]
$ve^-_{maxNO_3^-}$	The maximum cell-specific velocity of e^--flow to NO_3^-	9.34×10^{-15}	mol e^- $cell^{-1}$ h^{-1}	[18]
$ve^-_{maxNO_2^-}$	The maximum cell-specific velocity of e^--flow to NO_2^-	2.01×10^{-15}	mol e^- $cell^{-1}$ h^{-1}	[18]
ve^-_{min}	The minimum velocity of e^--flow to O_2/NO_x^-/NO_x required for protein synthesis (ATP)	1.95×10^{-17}	mol e^- $cell^{-1}$ h^{-1}	Assumption
$Ye^-_{O_2}$	The growth yield per mole of electrons transferred to O_2	4.97×10^{13}	cells (mol e^-)$^{-1}$	[18]
$Ye^-_{NO_x}$	The growth yield per mole e^- to NO_3^-, NO_2^-, NO, or N_2O	1.52×10^{13}	cells (mol e^-)$^{-1}$	[18]
Parameters common to both succinate and butyrate treatments				
$[O_2]_{na}$	The $[O_2]$ in aqua below which Nar production triggers	5.95×10^{-5}	mol L^{-1}	[18]
$[O_2]_{ni}$	The $[O_2]$ in aqua below which NirS production triggers	9.75×10^{-6}	mol L^{-1}	[18]
r_{Na}	The specific-probability for Nar production	0.035	h^{-1}	Optimisation
r_{Ni}	The specific-probability for NirS production	0.004	h^{-1}	Optimisation
ve^-_{maxNO}	The maximum cell-specific velocity of e^--flow to NO	3.56×10^{-15}	mol e^- $cell^{-1}$ h^{-1}	[33]
$ve^-_{maxN_2O}$	The maximum cell-specific velocity of e^--flow to N_2O	5.5×10^{-15}	mol e^- $cell^{-1}$ h^{-1}	[24]
K_{mO_2}	The half-saturation constant for O_2 reduction	2.25×10^{-7}	mol L^{-1}	Optimisation
$K_{mNO_3^-}$	The half-saturation constant for NO_3^- reduction	5×10^{-6}	mol L^{-1}	[34,35]
$K_{mNO_2^-}$	The half-saturation constant for NO_2^- reduction	4.13×10^{-6}	mol L^{-1}	[36,37]
K_{1NO}	The equilibrium dissociation constant for cNor/NO complex	8×10^{-14}	mol L^{-1}	[33]
K_{2NO}	The equilibrium dissociation constant for cNor/$(NO)_2$ complex	34×10^{-9}	mol L^{-1}	[33]
K_{mN_2O}	The half-saturation constant for N_2O reduction	5.93×10^{-7}	mol N_2O-N L^{-1}	Optimisation
D	Dilution (due to sampling): fraction of gas replaced by He	0.013–0.016	–	[18]
$k_{H(O_2)}$	Solubility of O_2 in water at 20°C	0.0014	mol L^{-1} atm^{-1}	[38]
$k_{H(NO)}$	Solubility of NO at 20°C	0.0021	mol L^{-1} atm^{-1}	[30]
$k_{H(N_2O)}$	Solubility of N_2O at 20°C	0.056	mol N_2O-N L^{-1} atm^{-1}	[38]
$k_{H(N_2)}$	Solubility of N_2 at 20°C	0.00035	mol N_2-N L^{-1} atm^{-1}	[38]
k_t	The coeff. for gas transport between headspace and liquid	3.6	L $vial^{-1}$ h^{-1}	Measured
O_{2leak}	O_2 leakage into the vial during each sampling	2.92×10^{-9}	mol	Measured
R	Universal gas constant	0.083	L atm K^{-1} mol^{-1}	–
T	Temperature	293.15	K	[18]
t_s	The time taken to complete each sampling	0.017	h	[30]
Vol_g	Headspace volume	0.07	L	[18]
Vol_{aq}	Aqueous-phase volume	0.05	L	[18]

doi:10.1371/journal.pcbi.1004621.t002

$\mathbf{K_{mO_2}}$ (Eq 17). *Pa. denitrificans* has three haem-copper terminal oxidoreductases [39] with K_{mO_2} ranging from nM to μM [40,41], so we decided to estimate the parameter value by optimising K_{mO_2} for the low $[O_2]$ treatments data. Vensim was used for the optimisation, where $K_{mO_2} = 2.25\times10^{-7}$ neatly simulated the O_2 depletion for both the succinate- and butyrate-supplemented treatments.

$\mathbf{K_{mN_2O}}$. *In vitro* studies of NosZ from *Pa. denitrificans* estimate the values for K_{mN_2O} = 5 μM at 22°C and pH 7.1 [42] and 6.7 μM at 25°C and pH 7.1 [43]. When our model was simulated with K_{mN_2O} in this range, given our empirically estimated $ve^-_{maxN_2O}$ [24], the simulated N_2O reached concentrations much higher than that measured (see Results/Discussion). A more adequate parameter value (= 0.6 μM) was found by optimising K_{mN_2O} in Vensim. The value is within the range determined for soil bacterial communities [44].

$\boldsymbol{ve^-_{maxO_2}}$ (Eq 17) could be estimated using the empirically determined cell yield per mole of electrons to O_2 ($Ye^-_{O_2}$, cells per mol e^-) and the maximum specific growth rate (μ, h^{-1}): $ve^-_{maxO_2} = \frac{\mu}{Ye^-_{O_2}}$. We are confident about the yields for the two C-substrates used, but the empirically determined μ for the butyrate treatments is suspiciously low (= 0.067 h^{-1}), providing $ve^-_{maxO_2} = 2.45\times10^{-15}$ mol e^- $cell^{-1}$ h^{-1}. Simulations with this value grossly underestimated the rate of O_2 depletion compared to measured, which forced us to estimate the parameter value by optimisation: $ve^-_{maxO_2} = 4.42\times10^{-15}$ and 4.22×10^{-15} mol e^- $cell^{-1}$ h^{-1} for the succinate- and butyrate treatments, respectively. These values give μ = 0.22 and 0.12 h^{-1}, respectively: for the succinate treatments, the value is very close to that empirically determined (= 0.2 h^{-1}); for the butyrate treatments, the value seems more realistic than 0.067 h^{-1}.

$\boldsymbol{ve^-_{min}}$ (Eqs 2, 5 and 7) is the per cell velocity of e^--flow to O_2 ($ve^-_{O_2}$) assumed to generate minimum ATP required for synthesising the initial molecules of denitrification enzymes. Since we lack any empirical or other estimations for this parameter, it is arbitrarily assumed to be the $ve^-_{O_2}$ when $[O_2]_{aq}$ reaches 1 nM. At this concentration, ve^-_{min} is determined by the Michaelis-Menten equation $\left(ve^-_{min} = \frac{ve^-_{maxO_2}\times[O_2]_{aq}}{(K_{mO_2}+[O_2]_{aq})}\right)$, using $ve^-_{maxO_2}$ and K_{mO_2} given above. The values obtained for the succinate- and butyrate-supplemented treatments = 1.96×10^{-17} and 1.87×10^{-17} mol e^- $cell^{-1}$ h^{-1}, respectively, which for both the cases is 0.44% of $ve^-_{maxO_2}$. To investigate the impact of ve^-_{min} on the model behaviour (r_{Na} and r_{Ni}, Eqs 1, 2, 4, 5, 6 and 7), sensitivity analyses were performed by simulating the model with ve^-_{min} corresponding to $[O_2]_{aq} = 5\times10^{-9}$, 5×10^{-10}, and 0 mol L^{-1} (see Results/Discussion).

Results/Discussion

Low probabilistic initiation of *nar* transcription, resulting in the fraction of the population with Nar < 100%

To test the assumption of a single homogeneous population with all cells producing Nar in response to O_2 depletion, we simulated the model with the specific probability for a Z^- cell to initiate *nar* transcription (r_{Na}) = 4 h^{-1}. This resulted in 98% of the cells possessing Nar within an hour (see Eqs 1–3). Evidence suggests that less than half an hour is required to synthesise denitrification enzymes [17,18], but an hour's time is assumed here to allow margin for error. The results show that, for all the treatments, the simulated NO_2^- production (mol $vial^{-1}$) grossly overestimates that measured (Fig 3).

To find a reasonable parameter value, we optimised r_{Na} for the 0% O_2 treatments, so that the simulated NO_2^- production matches that measured. The results (Table 3) suggest that a low probabilistic initiation of *nar* transcription (average r_{Na} = 0.035 h^{-1}) is adequate to simulate the

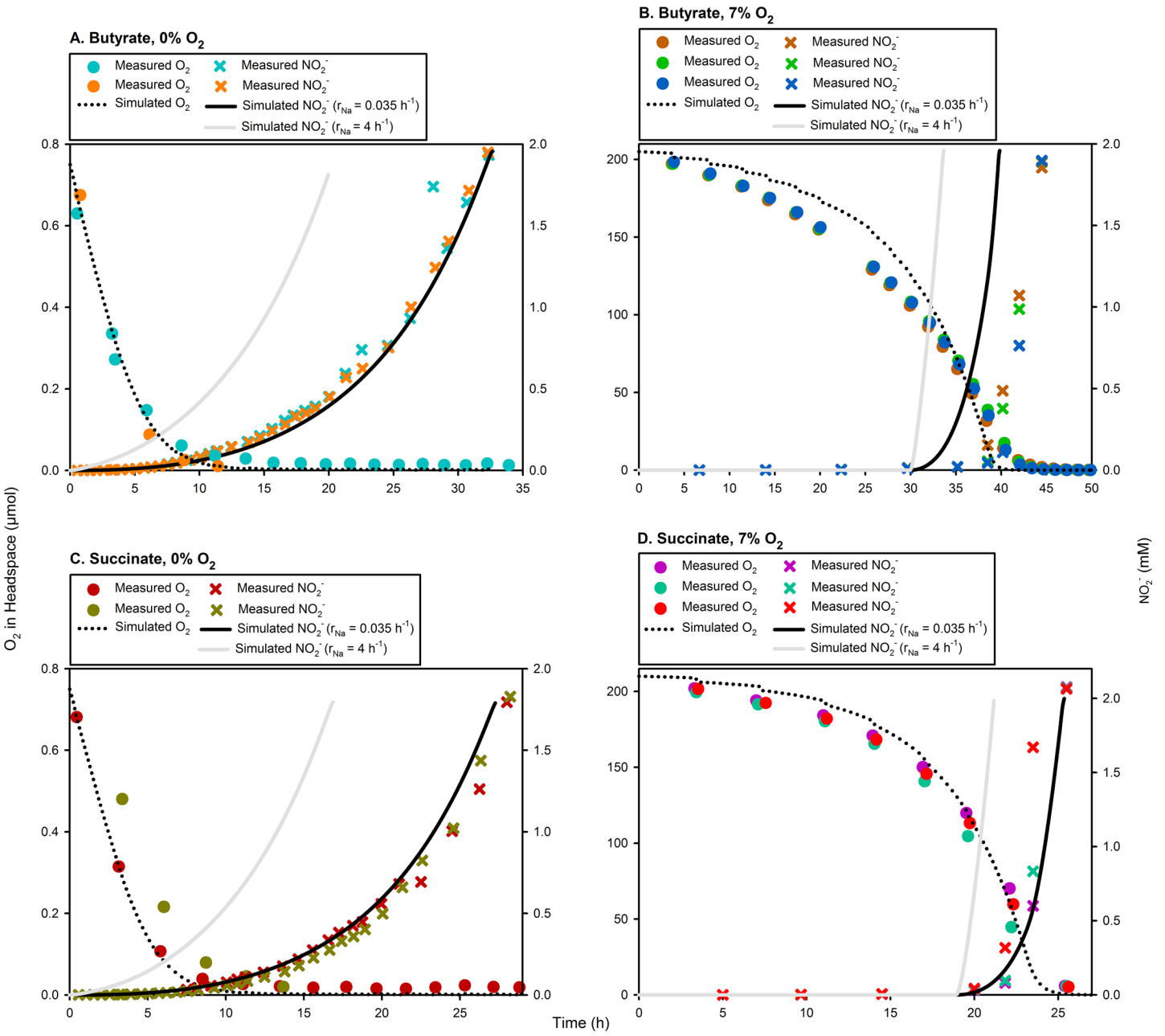

Fig 3. Comparison of measured and simulated NO_2^- accumulation assuming definitive versus stochastic initiation of *nar* transcription. To test the assumption of a single homogeneous population with almost all cells expressing *nar* in response to O_2 depletion, we forced our model to achieve 98% Nar-positive cells (Z^{Na}) within an hour by setting the specific-probability of initiating *nar* transcription (r_{Na}) = 4 h^{-1}. This resulted in grossly overestimated rates of NO_2^- accumulation for all treatments (grey curves). In contrast, we simulated the model with r_{Na} = 0.035 h^{-1} obtained through optimisation, resulting in a reasonable agreement with measurements for all treatments (except for an apparent time frameshift for the Butyrate, 7% O_2 treatment).

doi:10.1371/journal.pcbi.1004621.g003

measured NO_2^- kinetics (Fig 3). In the Butyrate, 7% O_2 treatment (Fig 3B), the simulated NO_2^- starts earlier, but the rate of accumulation is similar to that measured.

Once O_2 falls below a certain threshold, the production of Nar is assumed to trigger with r_{Na} = 0.035 h^{-1} and last until a minimum of respiration is sustained by the e^--flow to O_2 and N_2O ($ve^-_{O_2}$ and $ve^-_{N_2O}$), assumed to fulfil the ATP needs for Nar production (Eqs 1 and 2). But

Table 3. Specific-probability of *nar* and *nirS* transcriptional initiation (r_{Na} and r_{Ni}, respectively) estimated for each treatment by optimisation (best match between the simulated and measured data).

Batch	C-source	Treatment*: O_2 (vol.%), NO_3^- (mM)	Optimal r_{Na} (h^{-1})	Optimal r_{Ni} (h^{-1})
1	Butyrate	~0, 2	0.041	0.005
2	Butyrate	7, 2	–	0.004
3	Succinate	~0, 2	0.030	0.005
4	Succinate	7, 2	–	0.003
			Avg. = 0.035	**Avg. = 0.004**

*Treatment refers to the C-source, initial oxygen concentration in the headspace (measured as headspace-vol.%), and initial NO_3^- concentration in the medium (mM).

doi:10.1371/journal.pcbi.1004621.t003

the production of Nar sustained by $ve^-_{N_2O}$ was inconsequential for simulating the measured NO_2^- production, since NO_3^- was already exhausted when N_2O started accumulating (i.e., when $ve^-_{N_2O} > 0$). For this reason, the fraction that produced Nar (F_{Na}, Eq 3 and Table 4) is calculated as functional (= 0.23–0.43) and theoretical (= 0.56–0.81), where the first is the fraction actually responsible for NO_2^- production (sustained by $ve^-_{O_2}$), but the latter also incorporates the fraction that produced Nar after the exhaustion of NO_3^- (sustained by $ve^-_{O_2}$ as well as $ve^-_{N_2O}$). The rationale behind calculating the theoretical F_{Na} is the empirical data indicating that Nar transcription is not turned off in response to NO_3^- depletion [18]. Although our model cannot test the theoretical F_{Na}, but the functional F_{Na} suggests that, contrary to the common assumption, the measured NO_2^- kinetics can be neatly explained by only 23–43.3% of the population producing Nar in response to O_2 depletion.

Very low probabilistic initiation of *nirS* transcription

When we optimised the specific probability of *nirS* transcriptional activation (r_{Ni}, see Eqs 4, 5, 6 and 7) to fit the measured data, the average $r_{Ni} = 0.004\ h^{-1}$ (Table 3) adequately simulated the measured NO_2^- depletion and N_2 accumulation (Fig 4). The recruitment to denitrification lasted for 19.5–47.3 h, i.e., the time when $[O_2]$ was below a critical concentration and the velocity of e^--flow to O_2 and the relevant NO_x^-/NO_x remained above a critical minimum (Eqs 4, 5, 6 and 7). The resulting fraction recruited to denitrification (F_{Ni}, see Eq 8 and Table 4) was 0.08–0.18, the bulk of which depended on the e^--flow to NO_3^- and N_2O (instead of aerobic respiration).

To test whether the measured data could be explained without the recruitment sustained by NO_3^- and N_2O respiration, we also simulated the model with the recruitment as a function of

Table 4. The fraction of the population with Nar (F_{Na}) and NirS (F_{Ni}) estimated based on the optimal specific-probability of *nar* and *nirS* transcriptional initiation (r_{Na} and r_{Ni}), respectively.

Batch	C-source	O_2 (vol.%), NO_3^- (mM)	Functional F_{Na}* (unitless)	Theoretical F_{Na}* (unitless)	F_{Ni} (unitless)
1	Butyrate	~0, 2	0.433	0.813	0.221
2	Butyrate	7, 2	0.343	0.656	0.088
3	Succinate	~0, 2	0.357	0.803	0.206
4	Succinate	7, 2	0.230	0.564	0.077

*Functional F_{Na} is the fraction of cells expressing Nar while NO_3^- is still present, while Theoretical F_{Na} is the fraction expressing Nar when including the theoretical recruitment after NO_3^- depletion (supported by energy from N_2O reduction).

doi:10.1371/journal.pcbi.1004621.t004

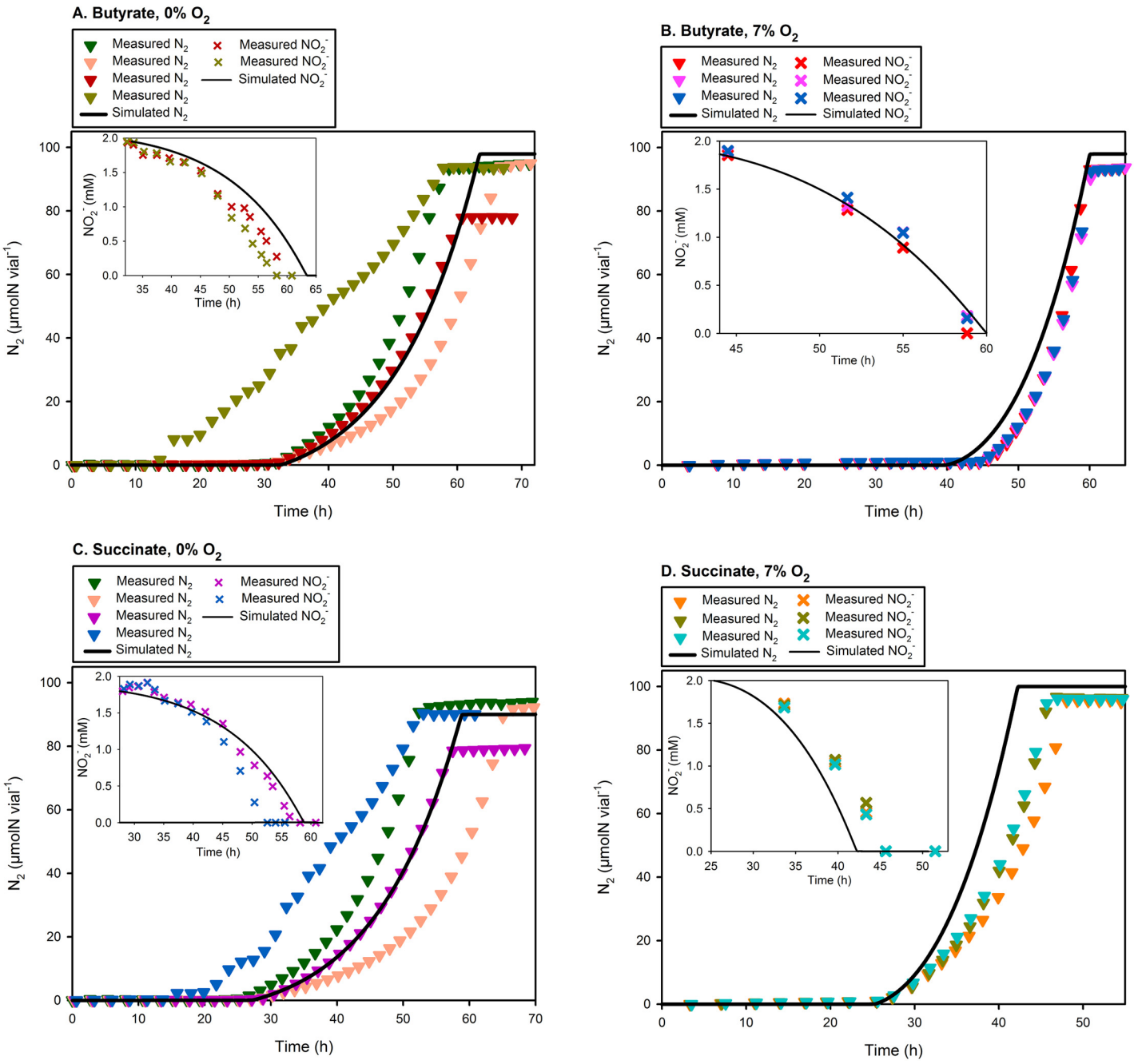

Fig 4. Comparison of measured and simulated data assuming stochastic initiation of *nirS* transcription. Each panel compares the measured NO_2^- depletion (sub-panel) and N_2 accumulation (main panel; n = 3–4) with simulations. The simulations are carried out with an optimised specific-probability of *nirS* transcriptional initiation (average r_{Ni} = 0.004 h^{-1}, Eqs 4, 5, 6 and 7), allowing 7.7–22.1% of the population to produce NirS + *c*Nor (Eq 8) during the available time-window (= 19.5–47.3 h).

doi:10.1371/journal.pcbi.1004621.g004

O_2 alone and re-optimised r_{Ni}, which on average increased to 0.012 h^{-1} (providing F_{Ni} = 0.083–0.35). This was expected since O_2 is exhausted rather quickly, shrinking the time-window available for the recruitment. Comparatively, these simulations were less satisfactory: using the average r_{Ni} = 0.012 h^{-1} generally resulted in larger deviations than for the default simulations (S2 Fig), and the optimal r_{Ni} for individual treatments varied grossly (50% higher values for the

Table 5. Estimated r_{Na} and r_{Ni}, depending on ve^-_{min}.

ve^-_{min} (mol e^- cell h^{-1})	Optimal r_{Na} (h^{-1})	Optimal r_{Ni} (h^{-1})
5 × Default*	0.041	0.0062
Default	0.035	0.0041
0.5 × Default	0.034	0.0035
0	0.033	0.0033

*Refers to the default value = 1.95×10^{-17} mol e^- $cell^{-1}$ h^{-1}.

doi:10.1371/journal.pcbi.1004621.t005

~0% O_2 treatments than for the 7% O_2 treatments). This contrasts the default simulations, where the optimal r_{Ni} values for individual treatments were quite similar.

Sensitivity of r_{Na} and r_{Ni} to ve^-_{min}

Recruitment to denitrification (both *nar* and *nirS* transcription) is assumed to continue only as long as the combined e^--flow to O_2, NO_3^- and N_2O is greater than ve^-_{min} (Eqs 1, 2, 4, 5, 6 and 7). To test the model's sensitivity to this parameter, we estimated r_{Na} and r_{Ni} by optimisation for different values of ve^-_{min}, relative to the default value = 1.95×10^{-17} mol e^- $cell^{-1}$ h^{-1}. For all cases, the model was able to adequately simulate the measured N_2 kinetics by moderate adjustments of r_{Na} and r_{Ni}. Table 5 shows the average optimal values of r_{Na} and r_{Ni}, obtained by fitting the simulated N_2 kinetics to the data, for different values of ve^-_{min}. S3 Fig shows adequate simulations of the measured N_2 kinetics assuming $ve^-_{min} = 0$, with optimised $r_{Na} = 0.033$ h^{-1} and $r_{Ni} = 0.0033$ h^{-1}. Thus, although assuming $ve^-_{min} > 0$ appears logical, it is not necessary to explain the measured data.

N_2O kinetics

To simulate the N_2O kinetics, we used $ve^-_{max N_2O} = 5.5\times10^{-15}$ mol e^- $cell^{-1}$ h^{-1}, empirically determined under similar experimental conditions as simulated here [24], and adopted the literature values for K_{mN_2O} [= 5 and 7 μM 42,43, respectively]. But with $K_{mN_2O} = 5$ μM, the model predicted N_2O accumulation ~10–20 times higher than measured for the ~0% and ~2–3 times higher for the 7% O_2 treatments (Fig 5). This forced us to simulate the model with the parameter value estimated by optimisation, providing the average $K_{mN_2O} = 0.6$ μM.

The measured N_2O shows a conspicuous increase throughout the entire active denitrification period, and this phenomenon is neatly captured by the model. The reason for this model prediction is that the number of N_2O producing cells ($Z^{NaNi} + Z^{Ni}$, Fig 2A) is low to begin with compared to the number of N_2O consuming cells ($Z^- + Z^{Na} + Z^{NaNi} + Z^{Ni}$), but the fraction of N_2O producers will increase during the anoxic phase for two reasons: one is the recruitment to Z^{NaNi} & Z^{Ni}, another is the fact that the model predicts approximately three times faster cell-specific growth rate for Z^{NaNi} & Z^{Ni} than for Z^- & Z^{Na} ($ve^-_{N_2O}$ is identical for all groups, while $ve^-_{NO_2^-}$ and ve^-_{NO} are both zero for Z^- & Z^{Na} but for Z^{NaNi} & Z^{Ni}, it holds that $ve^-_{NO_2^-} \approx ve^-_{NO} > ve^-_{N_2O}$. To illustrate this phenomenon, we ran the model, assuming that the Z^- & Z^{Na} cells had no N_2O reductase, resulting in *a)* constant N_2O concentration throughout the entire anoxic phase and *b)* much higher N_2O concentrations than measured (Fig 5). The overestimation is a trivial result, easily avoidable by increasing $ve^-_{max N_2O}$ or decreasing K_{mN_2O} moderately. However, the prediction of a constant N_2O concentration is clearly in conflict with the experimental

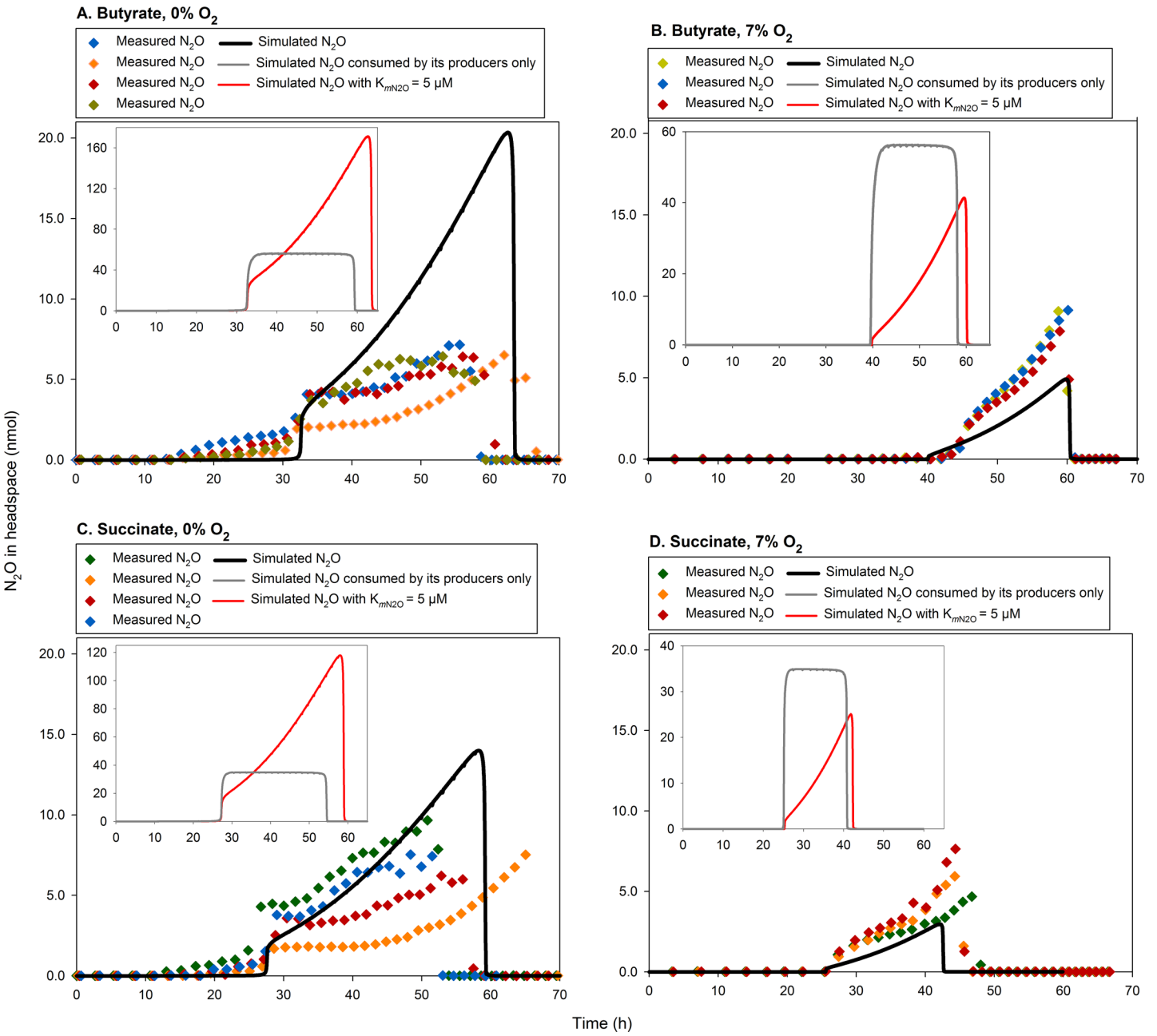

Fig 5. Comparison of the measured N_2O with that simulated. Each main panel (A–D) compares the measured N_2O (single vial results) with the default simulation using the parameter values given in Table 2, i.e., K_{mN_2O} = 0.6 µM (estimated through optimisation) and $ve^-_{maxN_2O}$ = 5.5×10^{-15} mol e^- $cell^{-1}$ h^{-1} [24]. In contrast, each inserted panel shows the simulated N_2O assuming 1) N_2O consumption only by the cells producing N_2O ($Z^{NaNi} + Z^{Ni}$), and 2) the literature value for K_{mN_2O} = 5 µM [42]. The results show that the default simulation best explains the measured N_2O kinetics, assuming its production by a small fraction ($Z^{NaNi} + Z^{Ni}$) and consumption by the entire population ($Z^- + Z^{Na} + Z^{NaNi} + Z^{Ni}$).

doi:10.1371/journal.pcbi.1004621.g005

data, and no parameterisation could force the model to reproduce this phenomenon other than the differential expression of denitrification genes.

Hence, although there is room for further refinements, our default assumption regarding differential expression of NirS and NosZ explains the observed N_2O kinetics: 1) abrupt initial accumulation to very low levels due to recruitment of relatively small numbers to the N_2O

producing pools (Z^{NaNi} & Z^{Ni}), and 2) increasing N_2O concentration due to recruitment and faster cell-specific growth of Z^{NaNi} & Z^{Ni} than that of the cells only consuming N_2O (Z^{-} + Z^{Na}).

This modelling exercise sheds some light on the possible role of regulatory biology of denitrification in controlling N_2O emissions from soils. If all cells in soils had the same regulatory phenotype as *Pa. denitrificans*, their emission of N_2O would probably be miniscule, and soils could easily become strong net sinks for N_2O because the majority of cells would be 'truncated denitrifiers' with only N_2O reductase expressed. It remains to be tested, however, if the regulatory phenotype of *Pa. denitrificans* is a rare or a common phenomenon among full-fledged denitrifiers. We foresee that further exploration of denitrification phenotypes will unravel a plethora of response patterns.

Conclusion

Using dynamic modelling, we have demonstrated that the denitrification kinetics in *Pa. denitrificans* can be adequately explained by assuming low probabilistic transcriptional activation of the *nar* and *nirS* genes and a subsequent autocatalytic expression of the enzymes. Such autocatalytic gene expressions are common in prokaryotes, rendering a population heterogeneous because of the stochastic initiation of gene transcription, with a low probability [45]. For N_2O kinetics, our hypothesis was that *a)* the gas is produced by a fraction of the incubated population that is able to initiate *nirS* transcription with a certain probability, leading to a coordinated expression of *nirS* + *nor* via NO [16], and *b)* N_2O is consumed by the entire population because, in response to anoxia, *nosZ* is readily induced by FnrP [24]. Our model corroborated this hypothesis by reasonably simulating the N_2O kinetics with the specific-probability of *nirS* transcriptional activation = 0.004 h^{-1}, resulting in 7.7–22.1% of the population producing NirS + *c*Nor (hence N_2O), but all cells producing NosZ (hence equally consuming N_2O).

Supporting Information

S1 Dynamic Model. The folder contains the dynamic model used in this study 'Hassan_et_al_2015_Pa._denitrificans.mdl'. The model requires Vensim (Double Precision), which is available at http://vensim.com/free-download/. The zip folder also contains files with the empirical data; these files are automatically loaded into the model when it is run.
(ZIP)

S1 Fig. *Pa. denitrificans* gas and NO_2^- kinetics. Typical gas kinetics (O_2, NO, N_2O, N_2) and NO_2^- accumulation in *Pa. denitrificans* during the transition from aerobic respiration to denitrification; batch cultures, n = 3; 20°C; Sistrom's medium; 2 mM KNO_3 and 7 vol% initial O_2 in the headspace. All the available NO_3^- (100 μmol $vial^{-1}$) was recovered as NO_2^- before the onset of N-gas production. In previous experiments [17], N_2O concentrations were below the detection limit of the system, but thanks to a new system with electron capture detector, the N_2O kinetics were monitored with reasonable precision. Adapted from [18].
(TIF)

S2 Fig. Comparison of measured and simulated data assuming stochastic initiation of *nirS* transcription with aerobic respiration being the only energy source for producing NirS + *c*Nor. In each panel, the measured NO_2^- depletion (sub-panel) and N_2 accumulation (main panel; n = 3–4) are compared with simulations. The simulations here are to be compared with the default simulations (Fig 4), which were run assuming that the coordinated NirS + *c*Nor production (via *nirS* transcriptional activation) is sustained by the energy generated by O_2 as well as NO_3^- and/or N_2O reduction. The default simulations provided an average specific-probability of *nirS* transcriptional activation (r_{Ni}) = 0.004 h^{-1} (Eqs 4, 5, 6 and 7) by optimisation,

allowing 7.7–22.1% of the population to produce NirS + *c*Nor (Eq 8) in 19.5–47.3 h. To match the measured data here, the average r_{Ni} had to be raised to 0.012 h^{-1}, since the time available for the enzyme synthesis shrank (= 3.5–16 h) due to a rapid exhaustion of O_2. Comparatively, the assumption that the ATP from NO_3^- and/or N_2O reduction should help cells produce denitrification enzymes seems more plausible and provide better agreement with the measured data.
(TIF)

S3 Fig. Measured vs. simulated N_2 kinetics assuming $ve^-_{min} = 0$. The default simulations are carried out assuming that for a cell to produce first molecules of Nar and NirS, a minimum of e^--flow to an available e^--acceptor (ve^-_{min}, mol e^- $cell^{-1}$ h^{-1}) is necessary to generate a minimum of ATP required for protein synthesis (Eqs 1, 2, 4, 5, 6 and 7). Although assuming $ve^-_{min} > 0$ seems logical, the measured N_2 kinetics are adequately simulated here with $ve^-_{min} = 0$. This shows that the assumption is not necessary to explain the measured data.
(TIF)

Author Contributions

Conceived and designed the experiments: LLB LRB. Performed the experiments: ZQ LLB. Analyzed the data: JH LRB. Contributed reagents/materials/analysis tools: JH. Wrote the paper: JH LRB.

References

1. Ravishankara AR, Daniel JS, Portmann RW (2009) Nitrous oxide (N_2O): the dominant ozone-depleting substance emitted in the 21st century Science 326: 123–125 doi: 10.1126/science.1176985 PMID: 19713491
2. Bates Bryson, Kundzewicz Zbigniew W., Wu Shaohong, Arnell Nigel, Burkett Virginia, et al. (2008) Technical paper on climate change and water. Budapest: Intergovernmental Panel on Climate Change
3. Lassey K, Harvey M (2007) Nitrous oxide: the serious side of laughing gas. Water & Atmos 15: 10–11.
4. Butterbach-Bahl K, Baggs EM, Dannenmann M, Kiese R, Zechmeister-Boltenstern S (2013) Nitrous oxide emissions from soils: how well do we understand the processes and their controls? Philos Trans R Soc Lond B Biol Sci 368: 20130122. doi: 10.1098/rstb.2013.0122 PMID: 23713120
5. Signor D, Cerri CEP (2013) Nitrous oxide emissions in agricultural soils: a review. Pesq Agropec Trop 43: 322–338.
6. Bakken LR, Bergaust L, Liu B, Frostegård Å (2012) Regulation of denitrification at the cellular level–a clue to understanding of N_2O emissions from soils. Philos Trans R Soc Lond B Biol Sci 367: 1226–1234. doi: 10.1098/rstb.2011.0321 PMID: 22451108
7. Bakken LR, Dörsch P (2007) Nitrous oxide emission and global changes: modelling approaches. In: Bothe H, Ferguson SJ, Newton WE, editors. Biology of the Nitrogen Cycle. Amsterdam: Elsevier B. V. pp. 382–395.
8. Bergaust L, Bakken LR, Frostegård Å (2011) Denitrification regulatory phenotype, a new term for the characterization of denitrifying bacteria. Biochem Soc Trans 39: 207–212. doi: 10.1042/BST0390207 PMID: 21265774
9. Zheng J, Doskey PV (2015) Modeling nitrous oxide production and reduction in soil through explicit representation of denitrification enzyme kinetics. Environ Sci Technol 49: 2132–2139. doi: 10.1021/es504513v PMID: 25588118
10. Betlach MR, Tiedje JM (1981) Kinetic explanation for accumulation of nitrite, nitric oxide, and nitrous oxide during bacterial denitrification. Appl Environ Microbiol 42: 1074–1084. PMID: 16345900
11. Vasiliadou IA, Siozios S, Papadas IT, Bourtzis K, Pavlou S, et al. (2006) Kinetics of pure cultures of hydrogen-oxidizing denitrifying bacteria and modeling of the interactions among them in mixed cultures. Biotechnol Bioeng 95: 513–525. PMID: 16758460
12. Almeida JS, Reis MAM, Carrondo MJT (1995) Competition between nitrate and nitrite reduction in denitrification by *Pseudomonas fluorescens*. Biotechnol Bioeng 46: 476–484. PMID: 18623340

13. Thomsen JK, Geest T, Cox RP (1994) Mass spectrometric studies of the effect of pH on the accumulation of intermediates in denitrification by *Paracoccus denitrificans*. Appl Environ Microbiol 60: 536–541. PMID: 16349183

14. Kampschreur MJ, Kleerebezem R, Picioreanu C, Bakken L, Bergaust L, et al. (2012) Metabolic modeling of denitrification in *Agrobacterium tumefaciens*: a tool to study inhibiting and activating compounds for the denitrification pathway. Front Microbiol 3.

15. Woolfenden HC, Gates AJ, Bocking C, Blyth MG, Richardson DJ, et al. (2013) Modeling the effect of copper availability on bacterial denitrification. Microbiologyopen 2: 756–765. doi: 10.1002/mbo3.111 PMID: 23913488

16. Hassan J, Bergaust LL, Wheat ID, Bakken LR (2014) Low probability of initiating *nirS* transcription explains observed gas kinetics and growth of bacteria switching from aerobic respiration to denitrification. PLoS Comput Biol 10: e1003933. doi: 10.1371/journal.pcbi.1003933 PMID: 25375393

17. Bergaust L, Mao Y, Bakken LR, Frostegård Å (2010) Denitrification response patterns during the transition to anoxic respiration and posttranscriptional effects of suboptimal pH on nitrogen oxide reductase in *Paracoccus denitrificans*. Appl Environ Microbiol 76: 6387–6396. doi: 10.1128/AEM.00608-10 PMID: 20709842

18. Qu Z (2014) Respiratory regulation in *Paracoccus denitrificans* and in soil, implications for N_2O emissions. Ås, Norway: Norwegian University of Life Sciences.

19. Bouchal P, Struhárová I, Budinská E, Šedo O, Vyhlídalová T, et al. (2010) Unraveling an FNR based regulatory circuit in *Paracoccus denitrificans* using a proteomics-based approach. Biochim Biophys Acta 1804: 1350–1358. doi: 10.1016/j.bbapap.2010.01.016 PMID: 20116460

20. van Spanning RJM, Richardson DJ, Ferguson SJ (2007) Introduction to the biochemistry and molecular biology of denitrification. In: Bothe H, Ferguson SJ, Newton WE, editors. Biology of the Nitrogen Cycle. Amsterdam: Elsevier B. V. pp. 3–20.

21. Wood NJ, Alizadeh T, Bennett S, Pearce J, Ferguson SJ, et al. (2001) Maximal expression of membrane-bound nitrate reductase in *Paracoccus* is induced by nitrate via a third FNR-like regulator named NarR. J Bacteriol 183: 3606–3613. PMID: 11371524

22. Spiro S (2007) Regulators of bacterial responses to nitric oxide. FEMS Microbiol Rev 31: 193–211. PMID: 17313521

23. Spiro S (2012) Nitrous oxide production and consumption: regulation of gene expression by gas-sensitive transcription factors. Philos Trans R Soc Lond B Biol Sci 367: 1213–1225. doi: 10.1098/rstb.2011.0309 PMID: 22451107

24. Bergaust L, van Spanning RJM, Frostegård Å, Bakken LR (2012) Expression of nitrous oxide reductase in *Paracoccus denitrificans* is regulated by oxygen and nitric oxide through FnrP and NNR. Microbiology 158: 826–834. doi: 10.1099/mic.0.054148-0 PMID: 22174385

25. Hutchings MI, Crack JC, Shearer N, Thompson BJ, Thomson AJ, et al. (2002) Transcription factor FnrP from *Paracoccus denitrificans* contains an iron-sulfur cluster and is activated by anoxia: identification of essential cysteine residues. Journal of bacteriology 184: 503–508. PMID: 11751828

26. Richardson D, Felgate H, Watmough N, Thomson A, Baggs E (2009) Mitigating release of the potent greenhouse gas N_2O from the nitrogen cycle–could enzymic regulation hold the key? Trends Biotechnol 27: 388–397. doi: 10.1016/j.tibtech.2009.03.009 PMID: 19497629

27. Bergaust L (2009) Regulatory biology of denitrification in *Agrobacterium tumefaciens* and *Paracoccus denitrificans*; responses to environmental controllers. Ås: Norwegian University of Life Sciences.

28. Nadeem S, Dörsch P, Bakken LR (2013) The significance of early accumulation of nanomolar concentrations of NO as an inducer of denitrification. FEMS Microbiol Ecol 83: 672–684. doi: 10.1111/1574-6941.12024 PMID: 23035849

29. Sistrom WR (1960) A requirement for sodium in the growth of *Rhodopseudomonas spheroides*. J Gen Microbiol 22: 778–785. PMID: 14447230

30. Molstad L, Dörsch P, Bakken LR (2007) Robotized incubation system for monitoring gases (O_2, NO, N_2O, N_2) in denitrifying cultures. J Microbiol Methods 71: 202–211. PMID: 17904668

31. Hannon B, Ruth M (2014) Modeling Dynamic Biological Systems; Ruth M, Hannon B, editors. New York: Springer

32. Girsch P, de Vries S (1997) Purification and initial kinetic and spectroscopic characterization of NO reductase from *Paracoccus denitrificans*. Biochim Biophys Acta 1318: 202–216. PMID: 9030265

33. Hassan J (2015) Exploring the regulation of denitrification and NO and N_2O kinetics in *Paracoccus denitrificans* using simulation modelling. Ås: Norwegian University of Life Sciences.

34. Parsonage D, Greenfield AJ, Ferguson SJ (1985) The high affinity of *Paracoccus denitrificans* cells for nitrate as an electron acceptor. Analysis of possible mechanisms of nitrate and nitrite movement across

the plasma membrane and the basis for inhibition by added nitrite of oxidase activity in permeabilised cells. Biochim Biophys Acta 807: 81–95.

35. Davies KJP, Lloyd D, Boddy L (1989) The effect of oxygen on denitrification in *Paracoccus denitrificans* and *Pseudomonas aeruginosa*. J Gen Microbiol 135: 2445–2245 2441. PMID: 2516869
36. Gates AJ, Luque-Almagro VM, Goddard AD, Ferguson SJ, Roldán MD, et al. (2011) A composite biochemical system for bacterial nitrate and nitrite assimilation as exemplified by *Paracoccus denitrificans*. Biochem J 435: 743–753. doi: 10.1042/BJ20101920 PMID: 21348864
37. Pan Y, Ni B- J, Yuan Z (2013) Modeling electron competition among nitrogen oxides reduction and N_2O accumulation in denitrification. Environ Sci Technol Lett 47: 11083–11091.
38. Wilhelm E, Battino R, Wilcock RJ (1977) Low-pressure solubility of gases in liquid water. Chem Rev 77: 219–262.
39. de Gier J- WL, Lübben M, Reijnders WNM, Tipker CA, Slotboom D- J, et al. (1994) The terminal oxidases of *Paracoccus denitrificans*. Mol Microbiol 13: 183–196. PMID: 7984100
40. Fukumori Y, Yamanaka T (1984) Two K_m values for cytochrome *c* of aa_3-type two-subunit cytochrome *c* oxidase from *Nitrobacter agilis*. FEBS Lett 170: 301–304.
41. Pitcher RS, Watmough NJ (2004) The bacterial cytochrome cbb_3 oxidases. Biochim Biophys Acta 1655: 388–399. PMID: 15100055
42. Kristjansson JK, Hollocher TC (1980) First practical assay for soluble nitrous oxide reductase of denitrifying bacteria and a partial kinetic characterization. J Biol Chem 255: 704–707. PMID: 7356639
43. Snyder SW, Hollocher TC (1987) Purification and some characteristics of nitrous oxide reductase from *Paracoccus denitrificans*. J Biol Chem 262: 6515–6525. PMID: 3032972
44. Holtan-Hartwig L, Dörsch P, Bakken LR (2000) Comparison of denitrifying communities in organic soils: kinetics of NO3- and N_2O reduction. Soil Biol Biochem 32: 833–843.
45. Raj A, van Oudenaarden A (2008) Nature, nurture, or chance: stochastic gene expression and its consequences. Cell 135: 216–226. doi: 10.1016/j.cell.2008.09.050 PMID: 18957198